Wear 322-323 (2015) 203–217

Contents lists available at ScienceDirect

Wear

journal homepage: www.elsevier.com/locate/wear

Tribological performance of laser peened Ti–6Al–4V

Dharmesh Kumar [a], Syed Nadeem Akhtar [b], Anup Kumar Patel [c], J. Ramkumar [b], Kantesh Balani [c,*]

[a] Materials Science Programme, Indian Institute of Technology Kanpur, Kanpur 208016, India
[b] Mechanical Engineering, Indian Institute of Technology Kanpur, Kanpur 208016, India
[c] Materials Science and Engineering, Indian Institute of Technology Kanpur, Kanpur 208016, India

ARTICLE INFO

Article history:
Received 10 September 2014
Received in revised form
15 November 2014
Accepted 17 November 2014
Available online 25 November 2014

Keywords:
Fretting
Other materials (Ti–6Al–4V)
Laser processing
Profilometry
Residual stress
Stick-slip.

ABSTRACT

Ti–6Al–4V is a well-known metallic biomaterial used for implants, but its use is limited by its inferior hardness and tribological resistance in vivo. Laser peening (LP) is one potential means to enhance its tribological properties. LP induces surface residual compressive stresses due to plastic deformation caused by the propagation of a shock wave. Further, performing laser peening under water can enhance a material's hardness and wear resistance because it confines shock waves to the surface of the material. In the current research, the influence of an excimer laser (Kr–F, 248 nm) with varying fluence on the fretting behavior of Ti–6Al–4V was carried out. An optimized laser fluence of 100 J/cm^2 resulted in an increase in hardness by 28% in air and 35% in water confining media, respectively, when compared to that of an untreated Ti–6Al–4V substrate. It was observed that the residual compressive stresses from LP increased from 540 MPa in air to 604 MPa in water. Fretting wear against bearing steel type AISI E52100 shows a major wear reduction on LP Ti–6Al–4V samples as wear volume decreased from 1.211×10^{-3} mm^3 to either 0.139×10^{-3} mm^3 or to 0.106×10^{-3} mm^3 in samples peened in air and water, respectively. Frictional hysteresis data show that the dissipation energy loss for Ti–6Al–4V substrate from 11.412×10^{-4} J is decreased to 3.284×10^{-4} J for LP sample at 20 N load. Moreover, a considerable fall in contact diameter is observed from the non-processed surface (0.29×10^{-3} μm) to the LP sample (0.176×10^{-3} μm). Friction log plots indicate that wear mechanisms are mostly adhesion, abrasion and delamination. Enhanced tribological performance of LP Ti–6Al–4V was observed using LP in a water medium, and indicates potential improvements when the alloy is used in joint replacements.

1. Introduction

Ti–6Al–4V is used in a variety of engineering applications due to its high strength, low density and high corrosion resistance, thus, withstanding dynamic loads and relative sliding, especially in turbine blades, aerospace vehicles and automotive components [1,2]. However, its potential applications are much broader, encompassing surgical tools and bio-implants. The only downside is its poor tribological characteristics such as release of metal debris due to friction during mobility, and release of metal ion that is toxic to human body [3]. Fretting wear occurs due to recurrent rubbing and slipping (in order of few micrometers) between two articulating surfaces [4]. Thus, in order to prevent the surface from degradation, surface modification techniques are mandated. Surface treatments that alter the microstructure of a surface include case hardening, shot peening, low plasticity burnishing, water jet peening and laser peening.

Laser peening (LP) is a proven surface treatment process to enhance the service life of engineering components operating under dynamic loads [5]. This process induces residual compressive stresses deep into the material surfaces, typically 5–10 times deeper than conventional metal shot peening. Thus, the generated residual compressive stresses (in order of several hundreds of MPa) prohibit the initiation and propagation of cracks and enhance its service life. Laser peening has been particularly efficient in enhancing the performance of components of aircraft engine and turbines [6].

Since mechanical fatigue generally occurs by the progressive growth of a surface crack under cyclic loading, then if the stress experienced at the crack tip is below that of critical stress intensity factor, then crack will cease to grow further and fatigue failure will not occur [7]. Laser peening process usually induces compressive stresses in the grains, increases the dislocation density, and also pins the crack propagation and dislocation movement, which is very beneficial in increasing the life of critical service components [8].

The concept of laser shock propagation for properties enhancement was first used in early 1960s by Fairand and Clauer [9],

* Corresponding author. Tel.: +91 512 259 6194.
E-mail address: kbalani@iitk.ac.in (K. Balani).

http://dx.doi.org/10.1016/j.wear.2014.11.016
0043-1648/

which was first practically demonstrated in 1970s, and subsequently patented by Dr. Phillip Mallozzi and Dr. Fairand of Battelle in 1974 [10]. Most of the work performed on LP used Q-switched laser pulses utilizes a very high wavelength 1064 nm or more, and there are only few studies on LP with low wavelength 248 nm. Since the absorption of laser by the material can be affected by the wavelength used, so excimer laser with 248 nm wavelength is utilized in the current work for better absorption [5].

In laser peening, the fluence of laser, the transparent overlay and the quality of coatings plays a vital role in improving the material performance, so experiments involve varying the laser fluence, the transparent overlay (water, air) and utilizing a coating (black paint). Fluence plays a critical role in laser peening process because higher the value of fluence higher the magnitude of shock pressure wave [11], which then develops intense residual compressive stresses on the surface of material [12]. The elastically deformed part of the component attempts to regain its original position, according to Hooke's law, but plastic deformation remains permanent. Therefore, the top layer of the target is subjected to compressive stress, whereas the area just below the surface is subjected to the tensile stress, maintaining equilibrium in the target without an applied external force. An increase in the compressive stress volume or magnitude is always associated with an increase in the tensile stress volume or its magnitude [9,10]. Thus, a significant advantage of the LP process is a higher depth of compressive stress when compared to that of other peening processes. The depth of compressive residual surface stress (σ_{surf}) is observed to be directly related to the depth of plastically affected zone (D_p) [13,14].

In the current work, commercially available titanium alloy (Ti–6Al–4V) is used because of its wide utility in the aerospace and automotive industries due to its low weight to strength ratio, good machinability and excellent mechanical and outstanding corrosion properties [15]. Moreover, due to its poor tribological characteristics, the mandate of surface modifications to result enhanced life in sliding and reciprocating applications is of much interest in the technical community [16]. So it is essential to modify surface characteristics via LP technique, and observe how the transparent overlay of air or water affects the tribological properties (i.e. fretting). The fretting damage is quantified via surface profilometry, and the damage accumulation via Hertzian contact is related through the contact diameter. Further, the energy dissipated per cycle is evaluated during fretting, and the friction-logs are generated to evince the damage mechanism (and corresponding wear volume and wear rate) in LP Ti–6Al–4V samples.

2. Experimental method

2.1. Materials and laser peening

Commercially available Ti–6Al–4V is selected with chemical composition (Ti-88.93, Al-6.73, V-4.34 atomic %) in the form of 1 mm sheet. Sheet was cut by diamond low speed saw into $1 \times 1\ cm^2$ size followed by mechanical polishing with 0.1 μm alumina and is cleaned through dipping samples in acetone. A Kr–F excimer laser (Coherent Variolas Compex Pro 205F) with repetition rates as high as 10 Hz and output pulse energy 505 mJ before attenuation (100 mJ) at 248 nm wavelength has been used. The laser beam spot size of $2 \times 2\ mm^2$ was maintained on the samples through the mask projection technique. The schematic diagram (Fig. 1) shows the experimental setup for underwater laser peening system in which the depth of transparent overlay was 2 mm and coating thickness was 4 μm on top surface.

Laser fluence is directly proportional to the pressure generation that is responsible for plastic deformation due to development of high magnitude compressive stresses, thus, producing high depth of penetration [17]. So a range of five values respectively $20\ J/cm^2$, $40\ J/cm^2$, $60\ J/cm^2$, $80\ J/cm^2$, and $100\ J/cm^2$ are chosen for the current study. Transparent overlay acts as confining medium of plasma, so parameters with different density such as water ($\rho = 999.97\ kg/m^3$) and air ($\rho = 1.225\ kg/m^3$) are selected in the current work [18]. A coating (water based black paint of thickness ~4 μm) is applied in order to prevent surface from intense melting and evaporation in the conducted experiments [19]. Nomenclature of LP samples is presented in Table 1.

2.2. Phase characterization

Phase characterization is performed on X-Ray Diffractometer (Bruker D8 focus) with Cu-Kα ($\lambda = 1.54060$ Å) as the incident x-ray wavelength. X-ray diffraction pattern of the material was analyzed by X'Pert HighScore Plus software. X-ray diffraction pattern of the material was analyzed by stripping off the Kα2 ($\lambda = 1.54443$ Å) from the material X-Ray diffraction pattern, FWHM (full width at half-maximum) value was calculated for every peak (from 30° to 70°). These values were used further for the calculation of residual strain and stresses by size-strain plot method. It is assumed that "strain profile" is Gaussian function and "crystalline size" is a Lorentzian function [14] through which strain and crystallite size can be calculated:

$$(d_{hkl}\beta_{hkl}\ \cos\ \theta)^2 = \frac{k}{D}(d_{hkl}^2\beta_{hkl}\ \cos\ \theta) + \left(\frac{\varepsilon}{2}\right)^2 \quad (1)$$

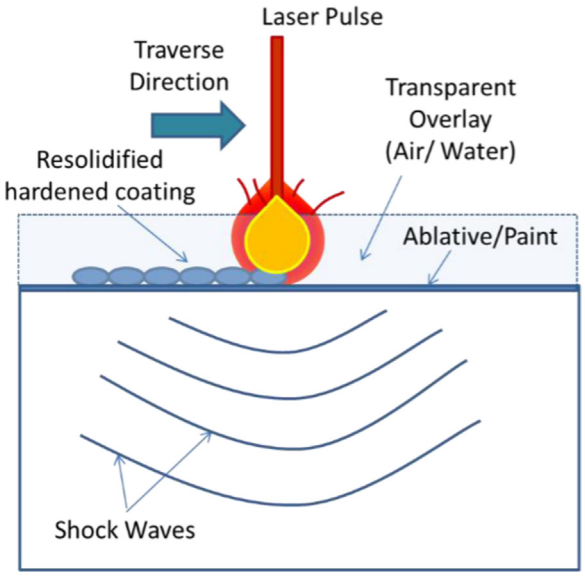

Fig. 1. Schematic diagram of laser peening, with transparent overlay being air or water.

Table 1
Nomenclature of the laser peened samples.

Nomenclature of laser peened samples				
Fluence (J/cm^2)	Without coating water air		With coating water air	
20	W20	A20	WC20	AC20
40	W40	A40	WC40	AC40
60	W60	A60	WC60	AC60
80	W80	A80	WC80	AC80
100	W100	A100	WC100	AC100

* The nomenclature "O" is used in the manuscript for untreated Ti–6Al–4V sample.

Fig. 2. Optical micrographs of microstructure (cross-sectional) of peened sample (a) A20 (b) A60 (c) A100 (d) W20 (e) W60 (f) W100 (g) AC20 (h) AC60 (i) AC100 (j) WC20 (k) WC60 (l) WC100. These laser peened samples elicited a minor change of microstructure with that of base material, and the depth values are also compared with that of hardness profiles shown later.

Table 2
Table of depth of penetration in laser peening.

Sample	Depth of penetration (μm)	Sample	Depth of penetration (μm)
A20	200	**W20**	250
A60	240	**W60**	270
A100	250	**W100**	300
AC20	200	**WC20**	210
AC60	220	**WC60**	250
AC100	230	**WC100**	270

where k is a constant ($=¾$ for spherical particles), d_{hkl} is inter-planar spacing, β is FWHM, D is an average crystalline size, and ε is the lattice strain.

2.3. Hardness measurement of laser peened samples

Micro-Vickers Hardness study was carried out using a Qualitest QV-10000 DM hardness machine system. In this system, hardness test was performed at the 25 gf load with a dwell time of 10 s. For

estimating the hardness along the transverse direction (i.e. from peened surface to bulk of material), the sample was cut, mounted and polished and indents were made traversing from surface to bulk.

2.4. Topography and tribological characterization

To investigate the effects of fretting wear on surface, fretting wear tests have been performed using reciprocating friction and wear monitor TR 281 M with Winducom 2006-upgrade software package. Chromium bearing steel (AISI E52100) sphere ball of diameter 6 mm has been used as counter body specimen at 10 Hz frequency and 100 μm displacement amplitude for 10,000 cycles at 10 N and 20 N load. Only one set of fretting test conditions was selected in order to test the effects of LSP within the capabilities of the current tribometer. Consequently, the use of other fretting test conditions might result in different behavior than the results presented in this focused study. Wear volume loss due to fretting wear is measured by optical surface profilometer (Bruker, Contour GT-1). Total of 51 lines at a distance of 40 μm in an area of 2 mm × 2 mm have been utilized to calculate the wear volume. Also, it must be pointed out that AISI E52100 is not an implant material, but fretting using this pin material will allow the comparison of fretting behavior with that of other data. Thus, the selection of AISI E52100 is not intended to simulate an actual implant material couple in which the counterface is likely to be other than bearing steel.

After fretting wear test, the oxide debris formed on the samples was manually cleaned using ethanol. For a thorough investigation, energy dispersive spectroscopy was utilized to analyze the elemental distribution on the fretted surface of the material. Surface roughness was measured by surftest (Mitutoyo, Japan), which displays the R_a and R_z values.

3. Results

3.1. Laser peening of Ti–6Al–4V with change of confining medium and ablative coating

The variation in the depth of penetration (D_p) with the varying fluence, different transparent overlays and the ablative coatings are shown in Fig. 2. The variation of D_p with the laser fluence in air (Fig. 2a–c) has shown an increase in depth of penetration from 200 μm to 250 μm in low (20 J/cm^2) and high fluence level (100 J/cm^2), respectively. Consequently, the depth of penetration changes from 250 μm to 300 μm when laser fluence, in the water medium, was changed from 20 J/cm^2 to high fluence of 100 J/cm^2, respectively. These results show that water serves as a better confining medium for plasma when compared to that of air (since the depth of penetration is 300 μm in water when compared to that of 250 μm in air as confining medium). The effect of ablative coating (black paint) is very marginal for both the confining mediums of air (Figs. 2 g–i) and water (Fig. 2j–l) i.e. coating thickness is still 230 μm in air, and 270 μm in water. Thus, in essence, it can be concluded that laser peening in water at high fluence (100 J/cm^2) is most efficient process for achieving a high depth of penetration. Correspondingly, Table 2 shows the depth of penetration with respect to depth from surface (according to change in slope) is illustrated at varying laser fluence and transparent overlays.

It is observed that laser peening treatment did not dramatically alter the average roughness of the sample (i.e. stays with R_a of 0.18–0.45), Fig. 3. Nonetheless, with LP in air as the medium, the laser is in directly contact with material, which results in high heat accumulation at surface (and thus marginally higher roughness). However, LP in water allows high heat dissipation due to its higher convection coefficient and results in a marginally lower roughness when compared to that of air. The generation of difference in topographic features due to non-uniform deformation and melting is not beneficial so surface is coated with black paint, which ablates very quickly upon exposure to the laser, and marginally reduces the net surface roughness in both the conditions, i.e., when confining medium is air or water.

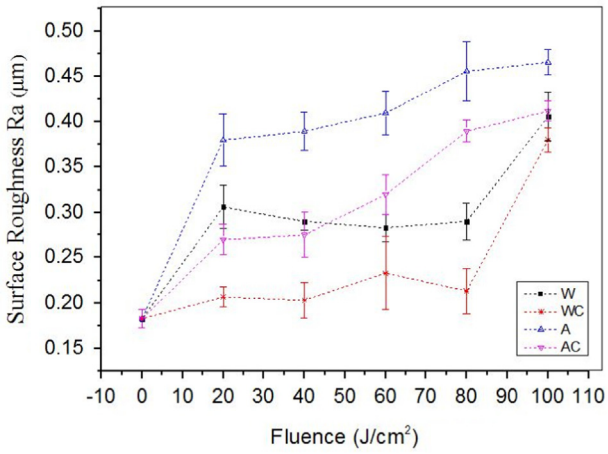

Fig. 3. Surface roughness at different fluences and media.

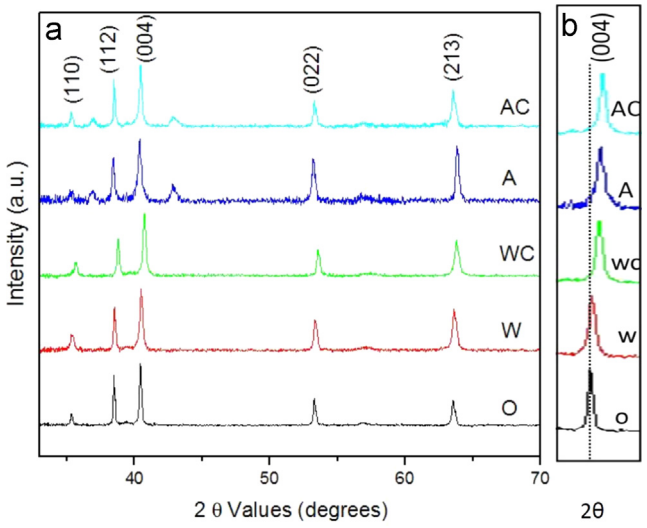

Fig. 4. X-ray diffraction pattern of: (a) the laser peened samples, and (b) magnified view showing the shift of (004) peak of samples processed at laser fluence of 100 J/cm^2. Letter O denotes untreated Ti–6Al–4V.

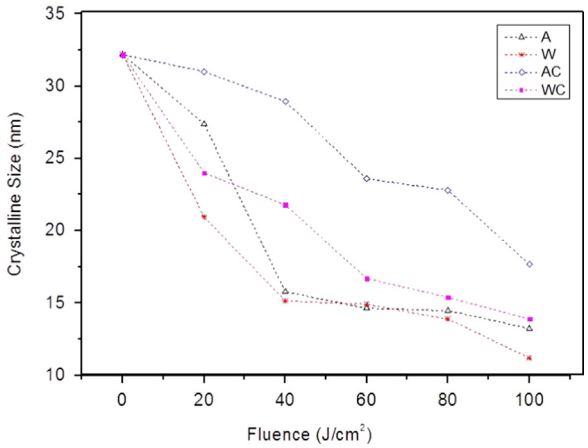

Fig. 5. Crystalline size with different laser fluence levels.

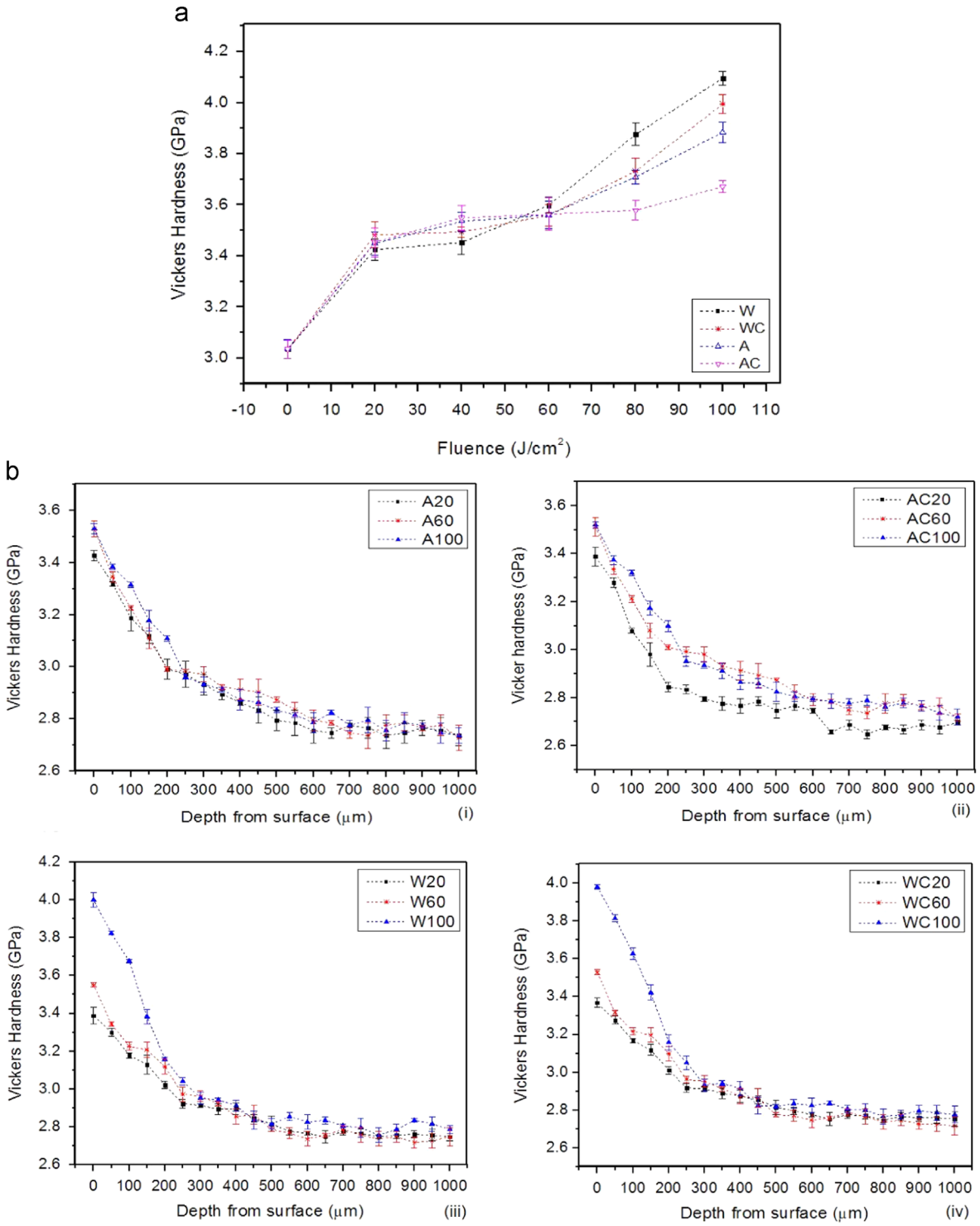

Fig. 6. Vickers hardness (a) in water and air medium varying fluence with and without coating, and (b) cross-sectional variation of hardness with laser fluence in various media (i.e. (i) in air, (ii) in air with ablative coating, (iii) in water, and (iv) in water with ablative coating).

3.2. *Phase characterization*

X-Ray diffraction does not show any formation of a new phase after laser peening, Fig. 4a. The shifting of peaks towards higher 2θ values can be easily observed from magnified view of (004) peak in Fig. 4b, indicating the presence of compressive residual stresses in the material.

The change in crystallite size as the function of laser fluence shows a decrease in the crystallite from ~32 nm to ~21 nm (in water) and ~28 nm (in air) at the laser fluence of 20 J/cm^2, which changes to ~13 nm (in air) and ~11 nm (in water) at the laser fluence of 100 J/cm^2. Moreover, the protective coating on the sample surface reduces the rate of reduction in crystallite size.

3.3. *Hardness and residual stresses in laser peened Ti–6Al–4V samples*

Upon laser peening, the Vickers hardness is observed to increase with the increasing laser fluence, i.e. the initial value of 3.03 GPa is increased to 3.42 GPa at 20 J/cm^2 and 4.09 GPa at 100 J/cm^2 in the

case of water transparent overlay. The same trend is followed in the confining medium of air, but the values are significantly lower than that of water medium, especially at higher laser fluence (see Figs. 5 and 6). The reduction of hardness to 3.99 GPa and 3.67 GPa in water and air at 100 J/cm^2, respectively, when the ablative coating is applied, is reasoned to the utilization of laser fluence in ablating the coating itself and not getting transferred into the material for its heating and resolidification. Overall statistics shows that the maximum increment in hardness value is achieved as 35% and 28% with water and air as confining medium, respectively.

Results also revealed that the change in hardness is significant within the penetration depth range of 200–300 μm, which, in turn, depends upon the fluence levels and the confining medium i.e. air/water and its thickness used in experiments (Fig. 2 and Fig. 6a).

In the depth profile of hardness (Fig. 6b), a significant change is observed with the change in laser fluence and the change in confining medium. Optimized results are obtained at a laser fluence of 100 J/cm^2 in water because the depth of penetration is 300 μm, which is much higher than that of the other samples. In case when ablative coatings are utilized, the depth of penetration is affected only at lower laser fluence (upto 60 J/cm^2). In air, the depth of penetration is significantly lower because of lower density of air is unable to confine shock waves into the material [20].

A residual compressive stress induced in the material with different processing parameters (laser fluence, transparent overlay, and coating) is shown in Fig. 7. It is revealed through analysis of X-ray diffraction pattern that compressive stresses increase with increasing laser fluence (Fig. 7). A compressive stress of 604 MPa and 336 MPa is achieved at the laser fluence of 100 J/cm^2 and 20 J/cm^2 in water, respectively. The same trend is followed when the confining medium is air, but the magnitude of residual compressive stress is significantly lower, i.e. 540 MPa and 264.6 MPa corresponding to laser fluence of 100 J/cm^2 and 20 J/cm^2, respectively. So by comparing both, the transparent overlay of water plays a prominent role to confine plasma during exposure to laser, inducing higher temperature and generating intense shock wave in the material to result higher plastic strain accommodation on material surface [5,14]. Thus, a higher magnitude of energy induces higher residual compressive stresses when the confining medium is water, and these effects are abated in the case of air as the confining medium, consequently the residual stress are significantly reduced at same laser fluence. In presence of the ablative coating, reduction in stresses has occurred to 551 MPa and 378 MPa at the laser fluence of 100 J/cm^2 in water and air, respectively, which arises as the propagation of shock wave is restricted resulting restricted deformation and, thus, lowering of the residual compressive stresses.

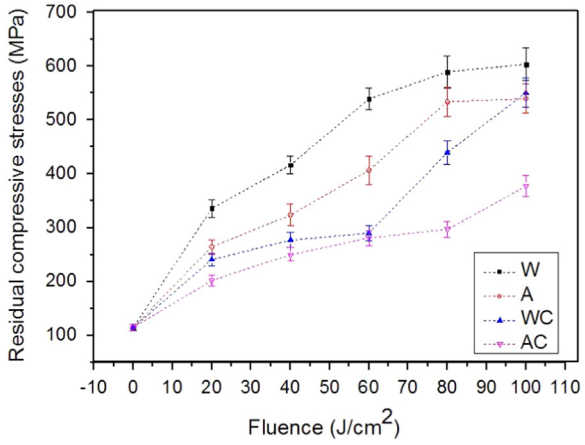

Fig. 7. Plot of the residual compressive stresses as the function of laser fluence.

3.4. Topography and tribological characteristics

Fig. 8a shows that the wear mechanism is primarily adhesive in untreated sample at 20 N load, where the sticking of surface material on the counter body is observed. The LP in air confining medium, Fig. 8b,c and d, at 20 J/cm^2 and 100 J/cm^2 laser fluence, respectively, show that the wear mechanism is majorly delamination but at 60 J/cm^2, wear mechanism has changed to abrasion. After laser peening in water medium, the damage mechanism stays adhesive but the formation of minute wear debris is also observed (Fig. 8e) at the surface. LP at laser fluence of 20 J/cm^2 in Fig. 8e shows an adhesion smearing on damage region, however LP with higher laser fluence of 60 J/cm^2 and 100 J/cm^2 show formation of wear groove on the fretting surface as observed in Fig. 8 f and g. Moreover, the shape of wear scar is also changing from circular to elliptical, which is presented as inset in Fig. 8b–g.

Delamination is observed in Ti–6Al–4V samples at the fretting load of 10 N, Fig. 9a. Though the wear mechanism remains delamination at laser fluence of 20 J/cm^2 in water and air confining medium (Fig. 9b and c), the wear volume is very less when compared to that of 20 N loading (Fig. 8).

Through optical profilometry, the scar wear profile of untreated sample and depth profile is measured to be 4.48 μm at 20 N load. The significant decrease in the surface wear profile of air laser peening and water laser peening are obtained with a scar depth of 4.2 μm and 2.25 μm, respectively (not shown here). This signifies that the laser peening in water is most effective in reducing fretting damage because wear volume (depth as well as surface area) is less as compared to that obtained after laser peening in air.

Wear scar volume calculated through optical profilometer in untreated sample is 1.21×10^{-3} mm^3, which is far more higher than that of peened sample, i.e. 1.39×10^{-4} mm^3 in air and 1.06×10^{-4} mm^3 in water at laser fluence of 100 J/cm^2 (See Fig. 10a). Decrease in wear volume with laser peening is attributed to a higher hardness (Fig. 6) and higher residual compressive stresses (Fig. 7) in water transparent overlay. Harder surface with high compressive stresses provide a better resistance against detachment of particles from one another, which is the reason that peening at lower laser fluence shows a high wear volume for A20 and W20 i.e. 4.95×10^{-4} mm^3 and 4.50×10^{-4} mm^3, respectively. Wear volume with both the overlays (i.e. air and water) do not vary much at same laser fluence level, thus it can be inferred that transparent overlay induce only marginal effect on the specific wear rate.

4. Discussion

4.1. Effect of laser fluence on tribological behavior of Ti–6Al–4V

In the initial increment of fluence, the hardness of material is observed to increase (Fig. 6(a)), so that a decrease in both plastic deformation and COF occur [21]. In addition to that of difference in texture and surface roughness (Fig. 3 confirmed through optical profilometry) is marginally increasing with fluence but COF is very sensitive to roughness rather than hardness [6]. Also, the initial formation of oxide layer (in order of few micrometer thickness) between mating surface act as solid lubricant and decreases the COF but formation of wear debris increase the COF. So oxidation layer formation is less at 20 J/cm^2 and 100 J/cm^2 (shown later) and also debris particles (plowing action) present (Fig. 8(b) and (e)) are sufficient to increase the COF. But, oxide layer formation is high when compared to other fluence values (shown later) so COF is very less at 60 J/cm^2 (Fig. 11) at a fixed 20 N load. A similar pattern is followed in both air and water medium LP. These effects are very insignificant in case of low load (10 N) because of reduced interactions of surface

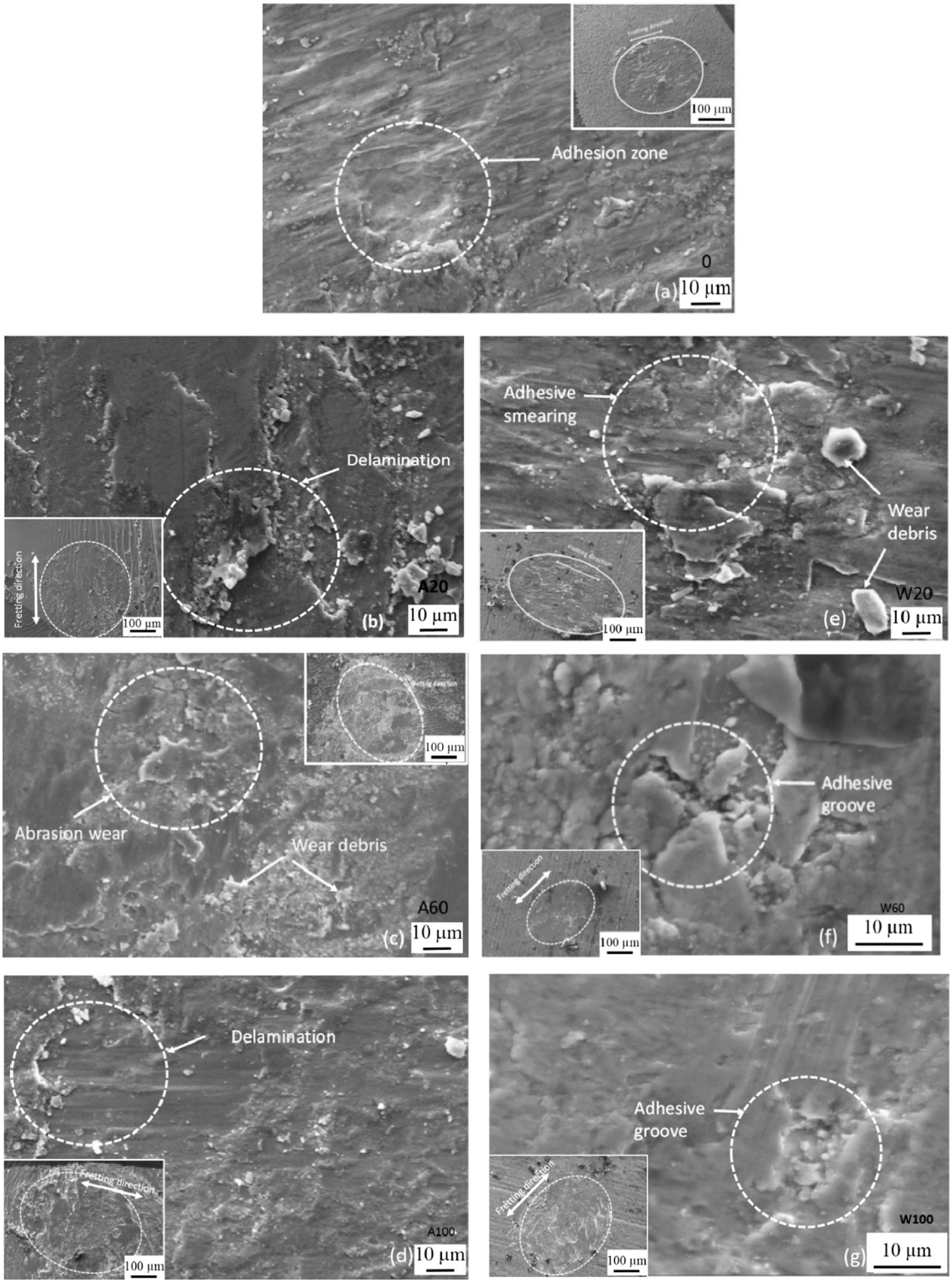

Fig. 8. SEM images of wear scars at different fluences at 20 N load (a) Original, O (b) 20 J/cm^2 in air, A20 (c) 60 J/cm^2 in air, A60 (d) 100 J/cm^2 in air, A100 (e) 20 J/cm^2 in water, W20 (f) 60 J/cm^2 in water < W60 (g) 100 J/cm^2 in water, W100 (Inset view is the demagnified view of wear scar).

with counter body (when compared to that at 20 N) and required prolonged duration to reach steady state condition.

SEM images confirmed that the shape of wear scar changed from circular to elliptical from a low load (10 N) to a high load (20 N) as shown in Fig. 8 and Fig. 9. Wear scar in optical profilometry shows an increase in depth as adhesion wear takes place at high load (20 N) because of proper contact (junction formation and interlocking of asperities) between mating surfaces. Relatively smooth surface is obtained at lower load and the damage surface at high load has occurred due to adhesion groove and smearing. At higher load, steady state condition is very easy to attain so higher wear volume is obtained via quantification through surface profiling, but at lower load, transition zone (actual contact area) is high so a lower wear volume is attained. The delamination mechanism is observed to occur as the result of detachment of wear particles on both original sample and peened

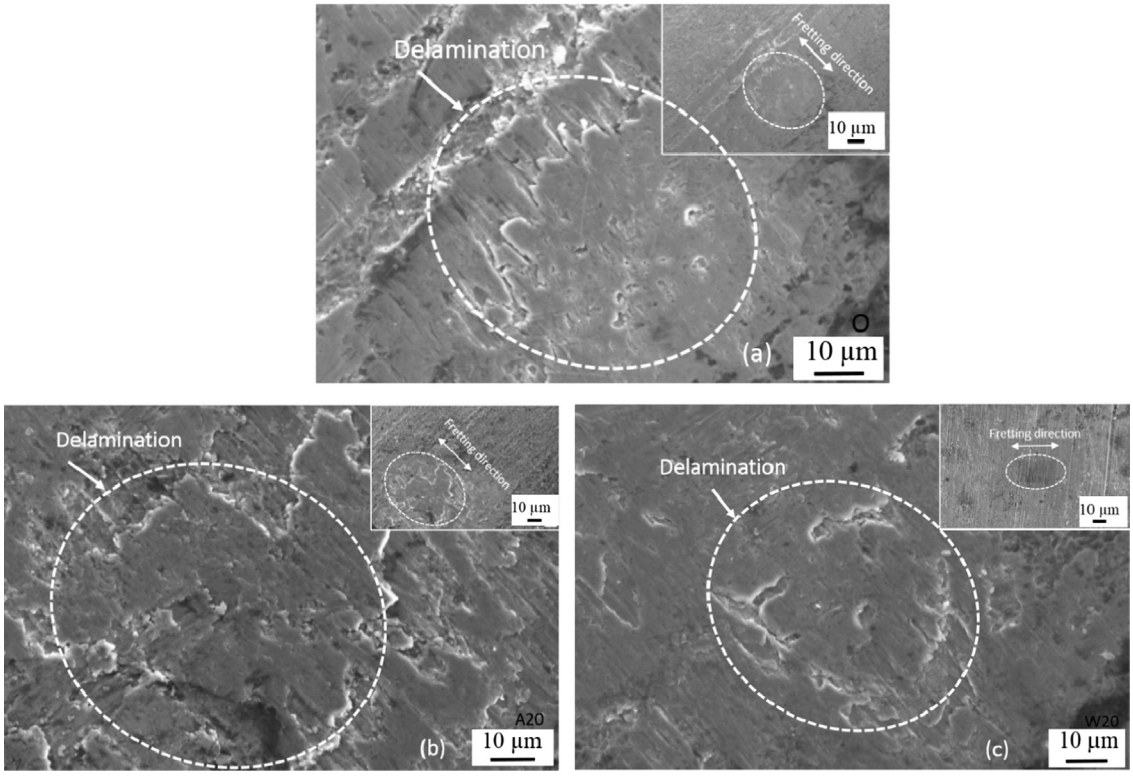

Fig. 9. SEM images of wear scars at different transparent overlays at 10 N load (a) Original (b) 20 J/cm^2 in air, A20, and (c) 20 J/cm^2 in water, W20.

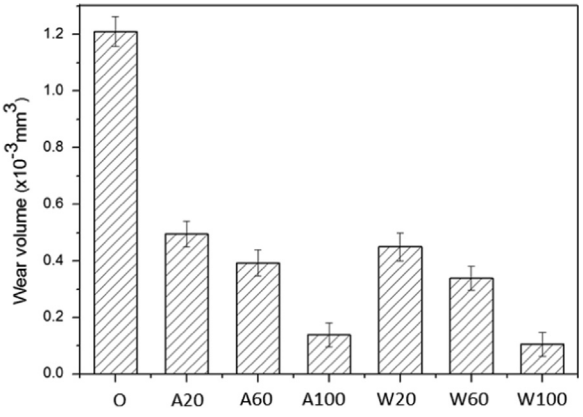

Fig. 10. Plot of wear volume at laser peening with different fluences.

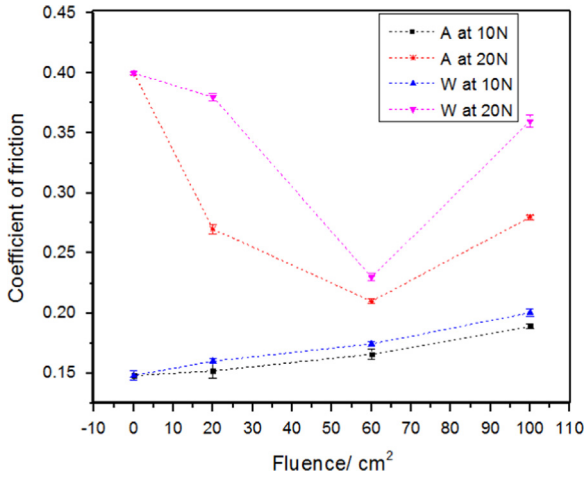

Fig. 11. Variation of COF of titanium at different normal loads (of 10 N and 20 N), at fixed stroke length of 100 μm, frequency 10 Hz, and 10,000 cycles.

sample at 20 J/cm^2 fluence when the sub-surface cracks generate during fretting to reach a critical length and break through to the surface. The most evident sign of delamination is the existence of debris particles (like plate), which is mainly generated by adhesion and metal-metal contact, which can also be produced by ratcheting (accumulation of unidirectional strain) [22]. During wear, the material at and very near the surface does not have a high dislocation density [23], due to the elimination of dislocations by the image force acting on those dislocations, which are parallel to the surface. Therefore, the final observed shape of the fretting damage is changing from circular to elliptical, which is dependent upon the fretting length and internal strains.

As already discussed, COF is less in case of air when compared to that of water at 10 N and 20 N load. At higher load, the effect of hardness is dominating as compared to roughness because of its close contact with the surface. Although hardness has little effect on friction, there is evidence that, in general, the friction is less with harder surface [24]. Experiments on titanium alloy show that the friction decreases linearly with the increasing hardness. For a given load, the amount of plastic deformation at the points of intimate contact is greater than that for a soft metal [25]. It is suggested that this deformation facilitates disruption of the oxide film so that for softer metals, the proportion of oxide-free junctions is greater [24]. The resulting frictional force is, therefore (due to large plastic deformation), higher. So for air LP, hardness is relatively low as compared to that of water laser peened surface so COF is lower in case of air LP. One more reason is attributed to the fact that the counter body interacts with surface peaks in air LP, so less COF is achieved.

SEM images (Fig. 8) and friction log of wear scars confirmed that there is very insignificant effect of the transparent overlay on the resulting wear scars. The only difference is that in water

medium, adhesive wear scars are dominant, but in air as confining medium, abrasion wear on surface is dominant. Grooves were created on the LP treated sample surface due to detachment of particles on counter body in water as confining medium, but in air medium, wear scar is large and uniform.

4.2. Effect of number of cycle on coefficient of friction

Coefficient of friction versus number of cycles plot shows an initial transient period followed by a steady-state regime (Fig. 12). The frictional force initially increases rapidly due to uneven contact between specimen and counterpart mating surface, and once perfect contact is achieved, it achieves a steady-state condition. The effect of hardening and accumulation of debris reasons for the transient behavior around ~0.06 as shown in Fig. 12a for O and shows an increasing trend from low laser fluence (20 J/cm^2) to high laser fluence (100 J/cm^2) in both air and water as confining media. The COF at 10 N load is 0.20 and 0.18 at high fluence (100 J/cm^2) for water and air respectively. The trend for COF is as follows in descending order:

$$O \approx W20 > W100 > A100 > W60 > A20 > A60 \text{ (20 N load)}$$

$$W100 > A100 > W60 > A60 > W20 > A20 > O \text{ (10 N load)}$$

COF value is increasing because of difference in texture though all coatings possess very similar R_a values [26]. However, it is possible that two different surface textures can have the same R_a, but their frictional characteristics could be different [26]. Roughness of all the confined sample falls within a band width of 0.18–0.45 μm which does not play any significant role in dictating the COF. In spite of similar roughness of water laser peening sample, COF is higher for air laser peening because of difference in surface texture due to intense melting and evaporation as surface temperature that can reach as high as 2200° C during laser peening (where the melting temperature of Ti–6Al–4V is 1604–1660° C) [15]. At the 20 N load (Fig. 12b), maximum COF occurs, since steady state condition is easily attained because contacting surface is relatively large (Hertzian contact diameter of 0.28 μm) when compared to that at lower load of 10 N (Hertzian contact diameter of 0.08 μm as computed later). So it provides a higher tangential force because of very uneven surface and asperities, and results higher COF value (0.40) at higher loads (20 N). The sudden inverse of COF takes place from 10 N to 20 N as hardness plays a dominant role at higher loads (in comparison to that of contact area) [27]. So it is better to predict that, for lower hardness materials, a good interaction occurs between two mating surfaces that allows smooth articulation or material transfers (deformation) from surface to counter body. This results in formation of a new layer and strengthening of surface that increase the shearing requirement, thus enhancing COF. In air, COF is low because the wear mechanism is abrasive, thus, generation of wear debris between the surface and the counter body does not affect the lateral force (or increase of COF).

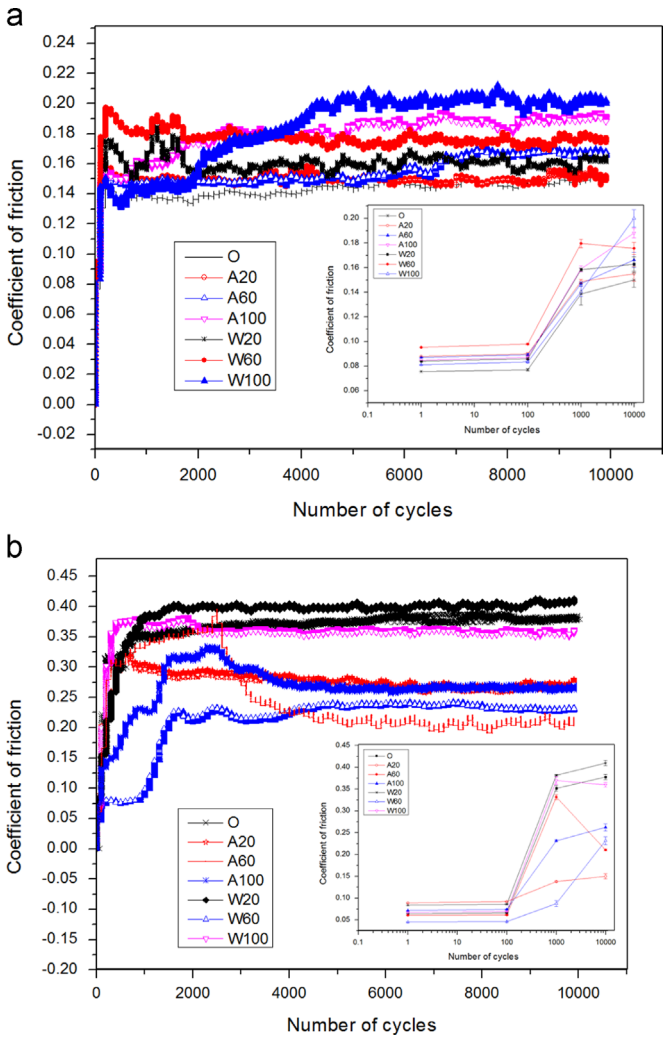

Fig. 12. Plot of coefficient of friction as a function of number of cycles for air and water with varying fluence at load (a) 10 N (b) 20 N (slip amplitude 100 μm, frequency 10 Hz). Inset shows logarithmic plot of coefficient of friction observed at various number of cycles.

The effect of tribo-oxidation is very significant in fretting wear, which is shown in elemental mapping (Fig. 13). Fretting induced damage in air is controlled by tribo-corrosion (more precisely tribo-oxidation of wear debris). With increase in load, contact area is observed to increase (Fig. 13), consequently, more wear debris is ejected, which readily oxidizes and abrades the surface. From SEM micrographs of wear scars, wear-scar volume is observed to increase and the shape (extent of tribooxidation) changes from circular to elliptical (as also observed in Figs. 8 and 9). Fig. 13 shows oxygen concentrations (using energy dispersive spectroscopy) at 20 N load and slip amplitude of 100 μm for Ti–6Al–4V at different fluence and transparent overlays, which confirms that adhesive fretting induces tribo-oxidation.

The effect of normal load on the fretting wear behavior of these alloys can be explained on the basis of Hertzian contact theory (contact pressure and stresses). Hertzian contact diameter (HCD) for ball (counter body) and flat (material, fretting behavior of which is of concern) configuration is given by

$$D = 2\left[\frac{3RF_n}{4E^*}\right]^{1/3} \quad \text{and} \quad \frac{1}{E^*} = \frac{1-\vartheta_1^2}{E_1} + \frac{1-\vartheta_2^2}{E_2} \tag{2}$$

F_n is normal load, R the ball (counter body) radius, E_i is Young's modulus, ν_i is the Poisson's ratio of the respective contacting materials. It is supposed in the Hertzian contact theory that contact stresses developed in the material are inversely proportional to the contact radius $\sigma_c = \sqrt{(1/R_c)}$, so that, in elastic region, HCD increment is beneficial. But, in the current case, plastic deformation of samples discards the validity of HCD theory. Nonetheless, Hertzian theory is applied just to point that the higher value of HCD is not desirable.

Hertzian contact diameter of unpeened Ti–6Al–4V is obtained to be 0.24 $\times 10^{-3}$ μm and 0.29 $\times 10^{-3}$ μm at 20 N and 10 N load, respectively (Fig. 14). HCD is 0.176 $\times 10^{-3}$ μm and 0.286 $\times 10^{-3}$ μm in water and air medium at 100 J/cm^2, also the trend is decreasing from low fluence (20 J/cm^2) to high fluence (100 J/cm^2) peening. It is because of HCD, which signifies the level of strain/stress at the point of contacts so as hardness is increasing with fluence, and, thus, HCD, is consequently decreasing.

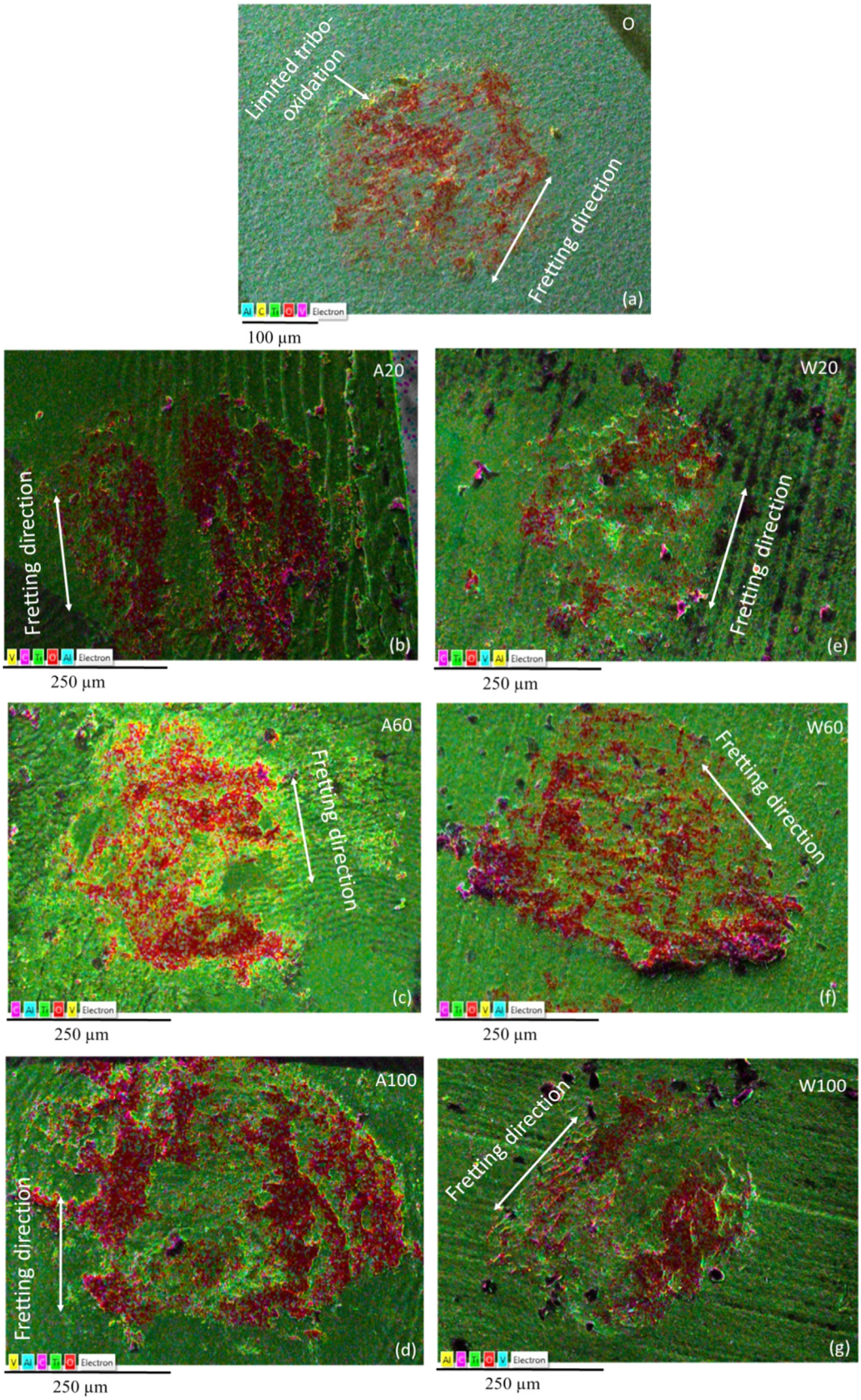

Fig. 13. Elemental mapping with fretting performed at 20 N load on samples (a) O (b) A20 (c) A60 (d) A100 (e) W20 (f) W60, and (g) W100.

As load increases, HCD is observed to increase, which causes increase in the area between counter body and the surface, which indicates that wear mechanism is changing from mild to severe. But, after laser peening, the wear volume is significantly reduced which is attributed to an increase in hardness (Fig. 6(a)) and the residual compressive stresses (Fig. 7). The plastically deformed zones are also

seen (Fig. 1) as the consequences of shock wave deformation via laser peeing. This residual compressive stress provides resistance to cracking and decrease of HCD with increasing laser fluence.

The shapes of friction hysteresis in all loading conditions and mediums are almost quasi-rectangular in shape at 100 μm stroke length (Fig. 15), which shows gross slip regime as the fretting damage mechanism. The extreme wavy circumference of hysteresis loop indicates sticking behavior over the entire stroke length of 100 μm. Area of the fretting hysteresis can be calculated by $A = \int Ft(D)ds$; where ds is the displacement amplitude, and the total area enclosed by friction hysteresis represents the dissipated friction energy during each fretting cycle. This dissipation energy gets stored in the material to promote thermo-mechanical induction, plastic flow and delamination under consideration or may transform into heat energy, which ultimately affects the wear volume during fatigue.

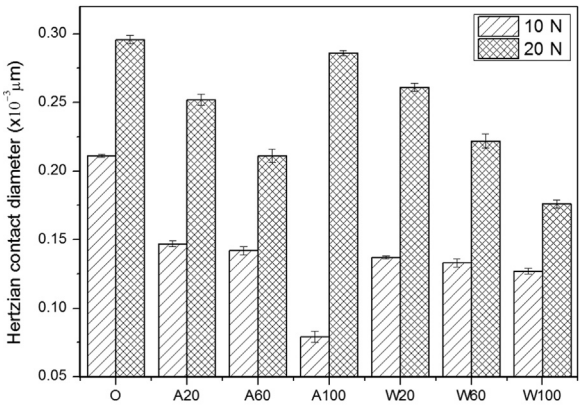

Fig. 14. Plot of Hertzian contact diameter with different fluence and medium.

As shown in Fig. 15, the untreated sample shows more hysteresis area when compared to the other laser peened samples, and also the hysteresis area increases at higher loading. Hysteresis loop area is observed to decrease as laser fluence is increased (Fig. 15 a and b), indicating that dissipation energy (causing wear) is lower after LP. Also, on comparing Figs. 15a and 15b, the hysteresis loop area is marginally small in water LP, which is attributed to higher dissipation energy in air when compared to that of water. Further, along the same line, enhanced fretting loading elicits increase in the friction hysteresis (Fig. 15c and d).

In fretting, applied normal load (F_N) acts on counter-body and undergoes reciprocating displacement (in order of few micrometers). The tangential force, which acts opposite to the direction of relative motion, i.e. the frictional force between two counteracting surfaces, can be calculated by:

$$F_S = \mu F_N \tag{3}$$

Sliding velocity can be given by $V = 2\nu\delta$

Where, μ is the coefficient of friction, δ is the displacement amplitude, and ν is the frequency of oscillation. Energy dissipated per cycle of fretting can be given by [28]:

$$U_f = 2\int_0^{\delta} F_s\, dr = 2F_S\delta = 2\mu F_N\delta \tag{4}$$

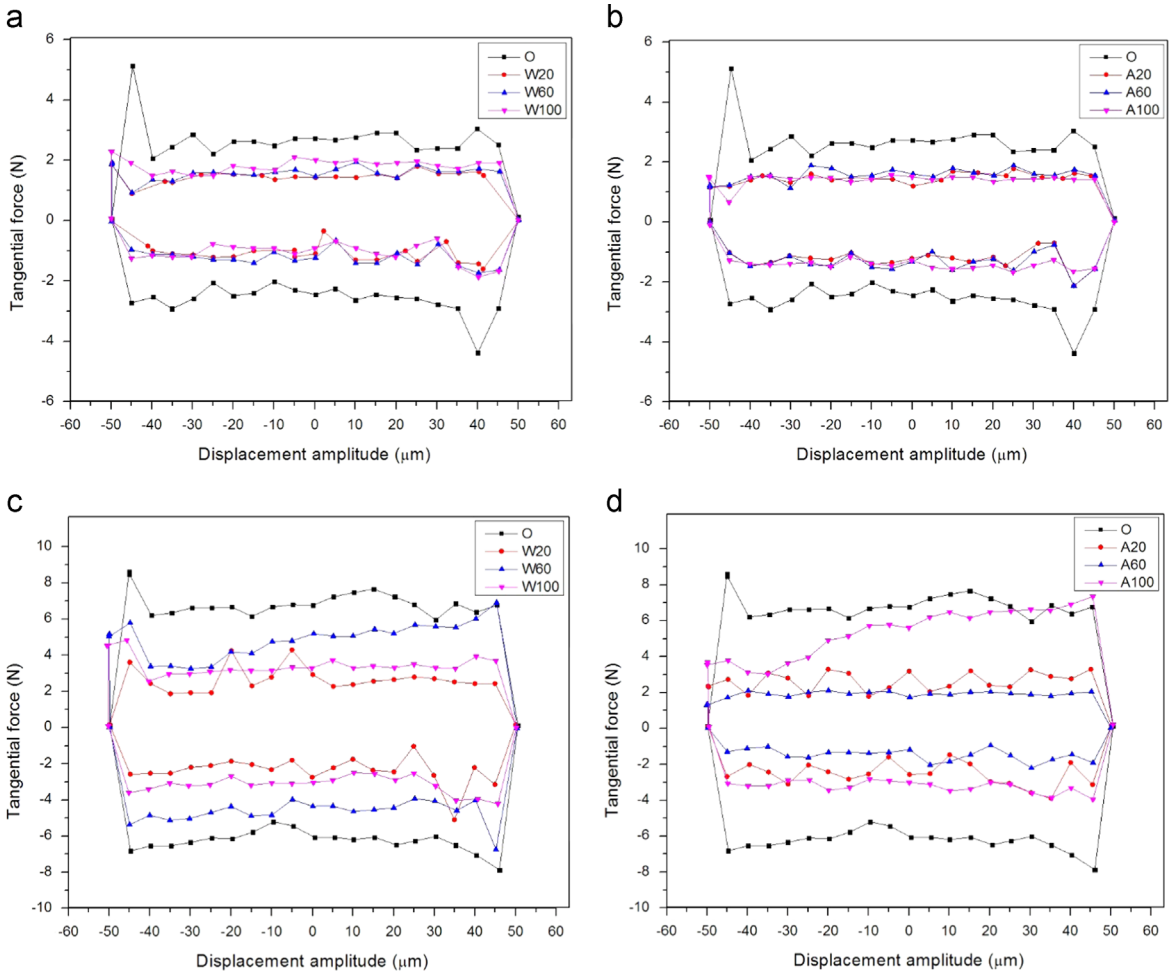

Fig. 15. Fretting hysteresis plot during test performed for 10,000 cycles, 10 Hz, 100 μm (a) W at 10 N (b) A at 10 N (c) W at 20 N (d) A at 20 N.

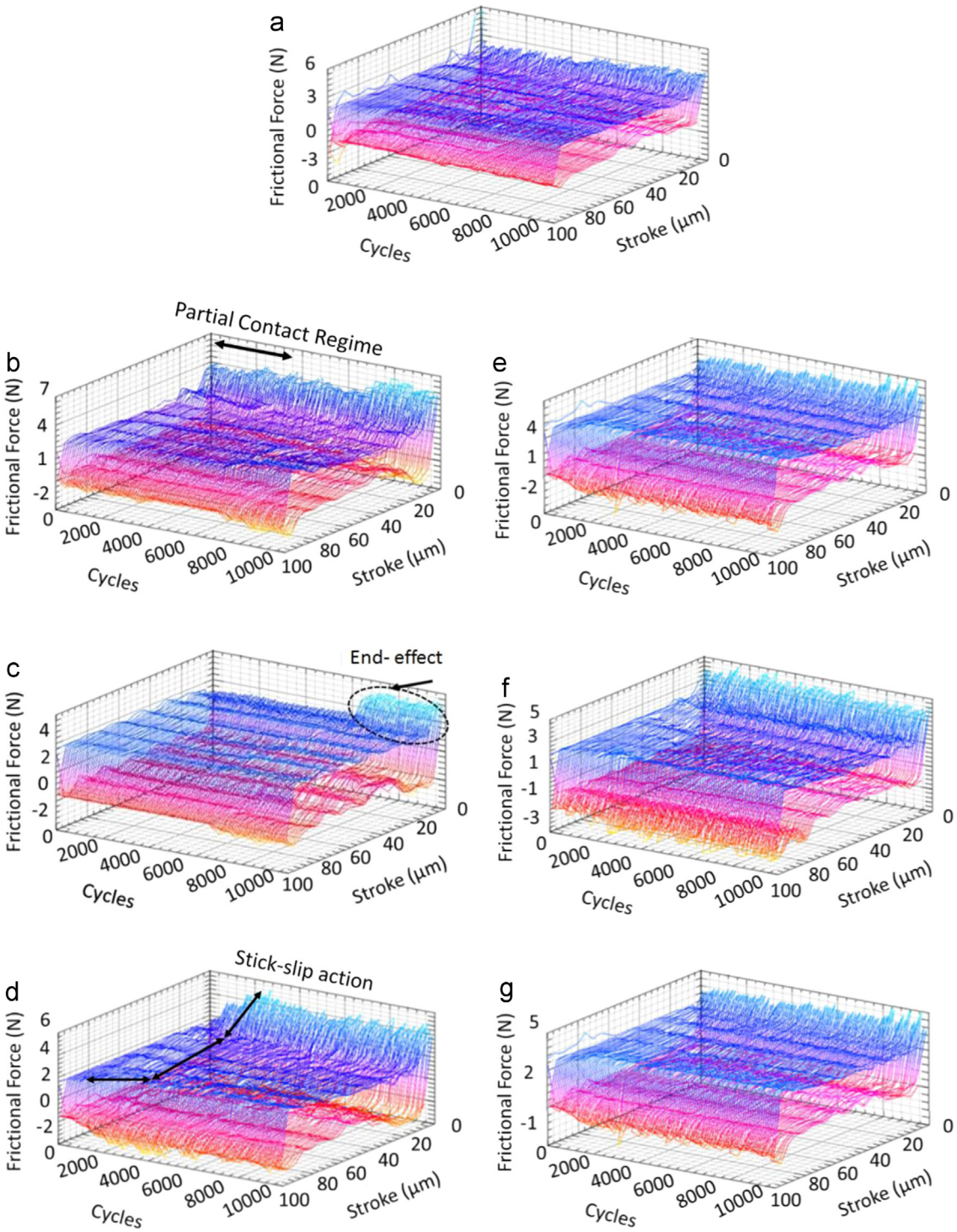

Fig. 16. Friction log of titanium alloy with frictional force (10 N), stroke (100 μm), cycles (number) is shown as legends. (a) O (b) A20 (c) A60 (d) A100 (e) W20 (f) W60 (g) W100.

where a factor of two is multiplied to accommodate the reciprocating nature in calculating the damage during fretting. The area under curve in between tangential force and displacement amplitude shows the dissipation energy, and as stated earlier, it can work either to deform the material surface or is released as the heat energy.

Friction log is a representation of frictional forces, displacement amplitude and number of cycles, which are helpful to analyze the transition and steady state zones and fretting condition proved among sticking, partial slip and gross slip. The linear nature of these curves shows sticking zone and rectangular nature validate the slipping behavior. These experiments are performed at certain conditions (Load 10 N and 20 N, displacement amplitude 100 μm, frequency 10 Hz), and the effect of load on different parametric conditions are shown as Figs. 16 and 17, and discussed. According to these plots (Figs. 16 and 17), frictional force is observed to be lower at 10 N load (Fig. 16) when compared to that at 20 N load (Fig. 17). Initially a transition zone is witnessed, which represents the intial interaction between the surface to counter body and later it becomes smooth as the interaction increases and makes the surface smoother.

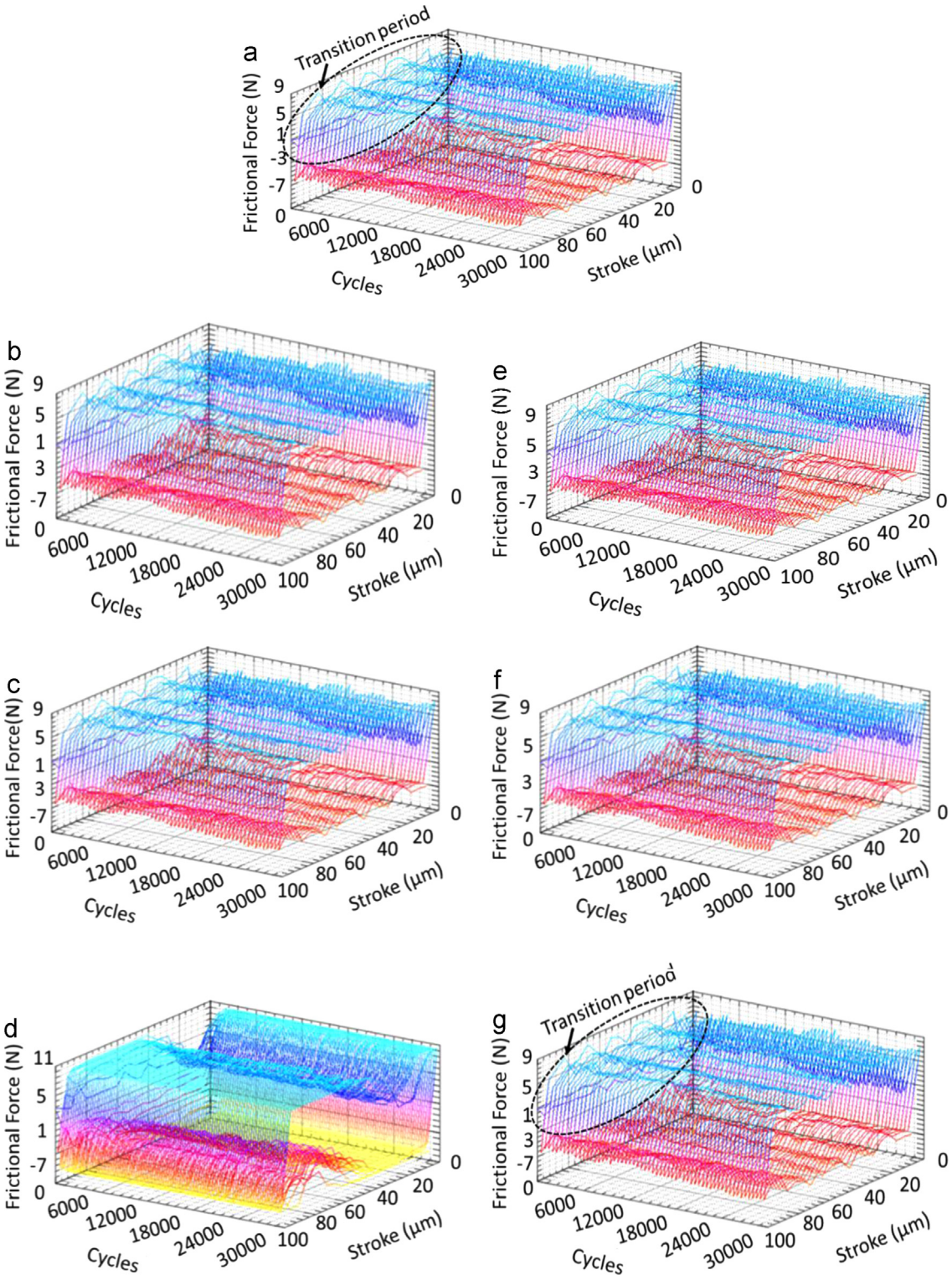

Fig. 17. Friction log of titanium at frictional force (20 N), stroke (100 μm), cycles (number) is shown as legends (a) O (b) A20 (c) A60 (d) A100 (e) W20 (f) W60 (g) W100.

Fretting logs for titanium alloy (Ti–6Al–4V) at 10 N load with varying fluence and confining medium are shown in Fig. 16. In these images, running-in period and transition period are marked, which reperesents an improper contact between the mating surfaces.

Fretting logs for titanium alloy (Ti–6Al–4V) at 20 N load with varying fluence and confining medium are shown in Figs. 16 and 17. When compared to low load (10 N), it can be observed (Figs. 16 and 17) that area under the curve is decreasing that represents lower wear and less energy consumption. Moreover the stick-slip phenomena is observed in the freeting logs at 10 N load Fig. 17d–g because of sudden change in the frictional force (sudden change in static and kinetic COF) which also causes vibration during contact. Also at high load (20 N), steady state is easily attained, and thus, stick slip phenomena is almost absent (Fig. 17a–g), which in turn, may also reduce the system vibration and noise.

In fretting logs, serrations present in coefficient of friction are due to the oscillations during fretting test. Initially, these oscillations under the action of high loads can be attributed to interaction with

surface asperities. At higher load (20 N), interaction with the surface asperities and consequent asperity damage is significantly higher than that at lower load (10 N). After completion of this running-in period, oscillation can be attributed to build up and accumulation of third body (wear debris) in contact region. Fig. 17b and c shows a partial contacting regime through which sudden increase in frictional takes place because of high wear asperities. In all cases, a parallogram indicates that accomodation of displacement occurs under the gross slip regime. In Fig. 16a, the rectangular shape of the friction log is very uniform because of low surface asperities and damage.

In-depth observation of the friction logs unveil that the coefficient of friction is relatively high at both ends in comparison to that at middle, which is attributed to the "end effect" microscopic wear scar images that impose hook effect to counter body under reciprocation motion [28]. The correlation of performed tribological and mechanical experiments is presented in Table 3. The results shows a correlation between hardness, HCD, COF, dissipation energy, wear volume and wear rate. Analysis of these results concludes that with the increment of hardness, HCD is decreasing because hard particles on the surface are resisting the contact between these mating surfaces. Similar trend is observed for dissipation energy as increment in hardness, where a sudden fall in dissipation energy takes place. Due to high hardness of laser peened surface, a rubbing effect is dominating instead of adhesion, irrespective of variation in the laser fluence.

Wear volume and wear rate of unpeened Ti–6Al–4 V sample is very high (1.211×10^{-3} mm^3), which is reduced to a very low value (0.106×10^{-3} mm^3) because of high hardness and presence of compressive residual stresses (Fig. 7) in water medium LP. Hardness plays a vital role in affecting wear volume because hard surfaces resist counter-body and limit the degree of surface damage/deformation. Hence, wear volume is reduced and also at high laser fluence that reduction in wear volume/wear rate is very large irrespective of confining medium. Coefficient of friction is decreased from the untreated sample (0.40 ± 0.0004) to that of the peened sample (0.21 ± 0.0002), which is attributed to a harder surface that promotes abrasive wear and reduced adhesive forces that minimize shearing force.

The schematic diagram in Fig. 18 shows the effect of laser fluence, transparent overlay, and ablative coating. In this shock wave, high confinement of plasma occurs in the water medium, but is comparatively shallow in the air confinement (Fig. 18a and b). In addition, coating act as protective layer from the intense surface melting of surface (Fig. 18c and d). These results indicate that LP of Ti–6Al–4V in water at 100 J/cm^2 has a great potential in the applications of automotive, bio-implants and aerospace industries due to its modified tribological properties.

Table 3
Correlation between materials properties in experiments at 20 N load.

Samples	Hardness (GPa)	HCD $\times 10^{-3}$ (μm)	Dissipation energy $\times 10^{-4}$ (J)	Wear volume $\times 10^{-3}$ (mm^3)	Sp. wear rate $\times 10^{-6}$ (mm^3/N-m)	COF
O	3.03	0.296	11.4	1.21	30.3	0.40
A20	3.44	0.252	4.83	0.495	12.4	0.27
A60	3.56	0.211	8.97	0.393	9.83	0.21
A100	3.88	0.286	6.35	0.139	3.48	0.28
W20	3.42	0.261	5.00	0.450	11.3	0.38
W60	3.59	0.222	3.28	0.339	8.48	0.23
W100	4.09	0.176	8.39	0.106	2.65	0.36

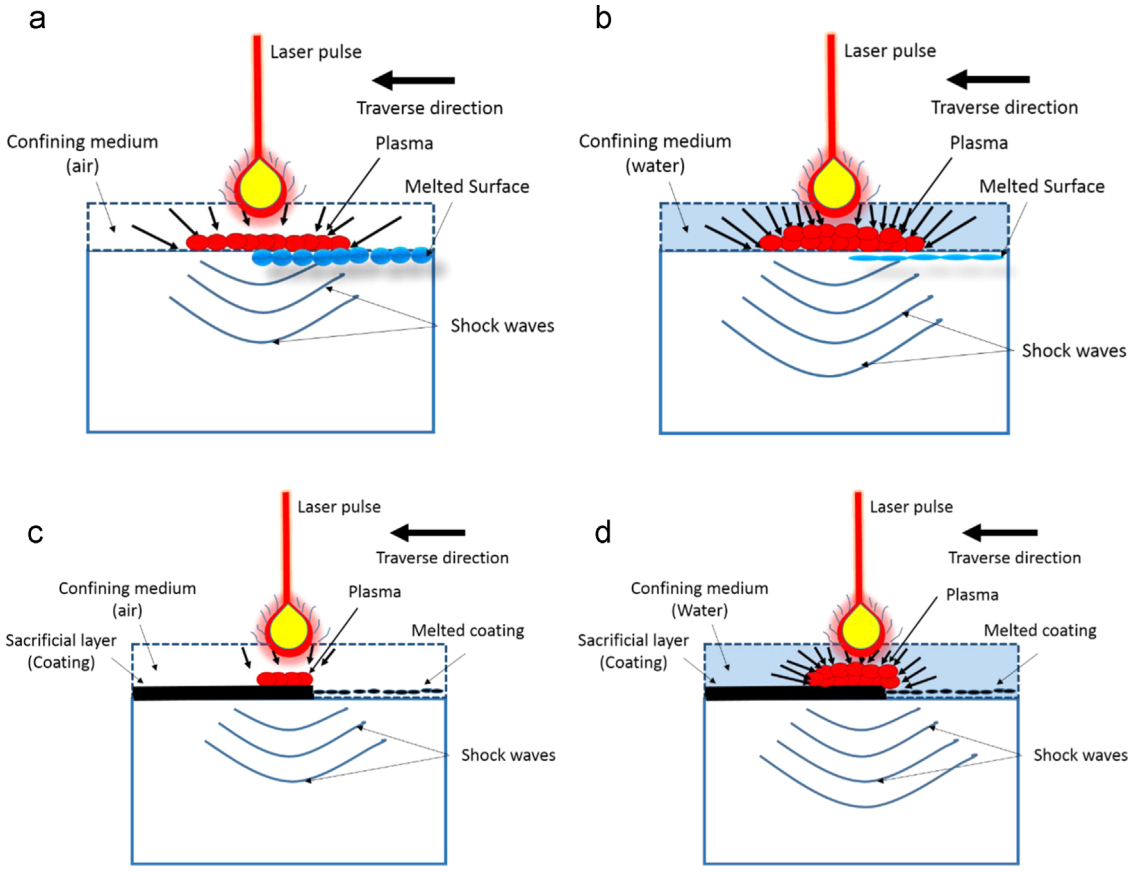

Fig. 18. Schematic diagram of laser peening at different parameters (a) A100 (b) W100 (c) AC100 (d) WC100.

5. Conclusions

An investigation of the effects of laser peening conditions on the fretting wear of Ti–6Al–4V against Type 52100 bearing steel has led to the following conclusions:

1. Surface hardness increases with the increasing laser fluence, which is optimized at 100 J/cm^2, for which, the surface hardness is obtained to be 3.88 GPa and 4.09 GPa in air and water medium, respectively. After using an ablative coating, a marginal reduction in the hardness is observed, which depict that the hardening of surface occurs in the presence of confining medium (without coating) to result in an enhanced tribological resistance.
2. At optimized laser fluence of 100 J/cm^2, compressive stresses in air medium are 540 MPa and 604 MPa in water. After using an ablative coating, a marginal reduction in the compressive residual stresses (i.e. to 378 MPa and 551 MPa in air and water, respectively) is obtained due to laser absorbance by coating. Compressive residual stresses are expected to enhance the fatigue life of the laser peened engineering components.
3. Mean COF is observed to increase with an increasing normal load (e.g. mean COF of O at 20 N load is 0.40 and at 10 N is 0.15). After laser peening, COF decreased at 20 N load because of the formation of a third body (oxide layer) when compared to that at 10 N load. The effect of the transparent overlay in affecting COF is very marginal, as for W20 and A20, COF is 0.165 and 0.155 at 10 N, and changes to 0.23 and 0.21 in W60 and A60 samples at 20 N load.
4. Overall fretting performance (at fixed displacement of 100 μm, frequency 10 Hz, and 10,000 cycles) is improved by the laser peening (wear volume reduced by 89% and 91% for A100 and W100, respectively, when compared to that of untreated sample). At the displacement amplitude of 100 μm, both oxidation and abrasion wear mechanism become active, and poor wear resistance is observed due to restricted increase in the hardness of the laser peened sample at laser fluence of 20 J/cm^2.
5. In fretting, wear gross slip region dominates, and friction log retained its rectangular or quasi-rectangular shape throughout sliding, which shows an absence of stick-zone formation. Higher COF observed in friction log can be attributed to the anchoring effect of the surface.

References

[1] L. Vincent, Materials and Fretting Fatigue, ESIS 18 EMP Ltd., London (1994) 323–337.
[2] B. Bhushan, B.K. Gupta, Handbook of Tribology: Materials, Coatings, and Surface Treatments, McGraw-Hill book company, New York (1991) 155–250.
[3] R. Boyer, G. Welsch, E.W. Collings, Materials Properties Handbook: Titanium Alloys, Vol. 42, ASM International, Materials Park, OH, USA (1994) 1339–1348.
[4] K.G. Budinski, Tribological properties of titanium alloys, Wear 151 (1991) 203–217.
[5] P. Payre, R. Fabbro, Laser shock processing: a review of the physics and applications, Opt. Quantum Electron 27 (12) (1995) 1213–1229.
[6] M.A. Meyers, Dynamic Behavior of Materials, John Wiley & Sons, Inc., New-York, USA, 1994.
[7] C.S. Montross, Tao Wei, Lin Ye, Graham Clark, Yiu-Wing Mai, Laser shock peening and its effects on microstructure and properties of metal alloys: a review, Int. J. Fatigue 24 (2002) 1021–1036.
[8] D. See, D.L., and R. Tenaglia, Affordable Laser Peening, In: Proceedings of the 8th National Turbine Engine High Cycle Fatigue Conference, Monterey, CA, (2003).
[9] E.M. Moroz, G.A. Askaryan, Effects of a laser beam in a liquid, Soviet Physics JETP USSR 17 (1963) 1463–1465.
[10] P.J.M.a.B.P. Fairand, Altering material properties. U.S patent 3850698 26 November 1974.
[11] C. Ye, Y.L., G.J. Cheng, Warm laser shock peening drivennano-structures and their effects on fatigue performance in aluminum alloy 6160, Adv. Eng. Mater. 12 (4) (2010).
[12] H. Kolsky, Stress waves in Solids, Dover Publications, New York, NY (1963) 177–178.
[13] P. Ballard, Contraintes residuelles induites par impact rapide (PhD Dissertation), Ecole Polytechnique, Paris, France, 1991.
[14] P. Ballard, J. Fournier, R. Fabbro, J. Frelat, Residual stresses induced by laser-shock, J. Appl. Phys. III 1 (c3) (1991) 487–494.
[15] J.M. (Tim) Holt (Ed.), Structural Alloys Handbook, CINDAS/Purdue University, West Lafayette, IN, 1996.
[16] J. Qu, P.J. Blau, T.R. Watkins, O.B. Cavin, N.S. Kulkarni, Friction and wear of titanium alloys sliding against metal, polymer, and ceramic counterfaces, Wear 126 (258) (2004) 1348–1356.
[17] J. Ihlemann, B. Wolff, P. Simon, Nanosecond and femtosecond excimer laser ablation of fused silica, J. Appl. Phys. A 54 (1992) 363–368.
[18] V.A. Ageev, A.F.B., V.V. Zhukovskii, A.A. Yankovskii, Dynamics of processes occurring in laser ablation of metals in a liquid, J. Appl. Spectr. (1997) 64.
[19] U. Trdan, A. Juan, Jose L. Porro, Janez Grum Ocana, Laser shock peening without coating(LSPwC) effect on 3D surface topography and mechanical properties of 6082-T651 Al alloy, Surf. Coat. Technol. 208 (2012) 109–116.
[20] S. Zhu, Y.F Lu, M.H. Hong, X.Y. Chen, Laser ablation of solid substrates in water and ambient air, J. Appl. Phys. 89 (4) (2001) 2400.
[21] G.W. Stachowiak, A.W. Batchelor, Engineering Tribology, fourth edition, Butterworth–Heinemann, UK (2013) 525–540.
[22] V. Swaminathan, J.L.G., Fretting corrosion of CoCrMo and Ti–6Al–4V interface, Biomaterials 33 (2012) 5487–5503.
[23] R.B Waterhouse, Residual stresses and fretting, crack initiation and propagation, volume IV 87132, Nottingham, UK.
[24] D.H. Buckley, Surface Effects in Adhesion, Friction, Wear and Lubrication, Elsevier, Amsterdam (1981) 220–230.
[25] A.J.W. Moore, W.J. McG. Tegart, Relation between friction and hardness, Proceeding of royal society of london. Mathematical and Physical Sciences, Vol 212, Issue 1111, pp.452–458.
[26] P.L. Menezes, Kishore, S.V. Kailash, Influence of roughness parameters on coefficient of friction under lubricated conditions, Sadhana 33 (3) (2008) 181–190.
[27] Gerhard Welsch, Rodney Boyer, E.W. Collins, Material Properties Handbook: Titanium alloys, ASM International,pp. 101–112.
[28] K. Sikdar, S. Shekhar, K. Balani, Fretting wear behavior of thermomechanically processed Mg–Li–Al based alloys, Wear 318 (1–2) (2014) 177–187.